Title

Pharmacological inhibition of soluble epoxide hydrolase provides cardioprotection in hyperglycemic rats

Journal

AJP Heart and Circulatory Physiology, 303(7)

ISSN

0363-6135

Authors

Guglielmino, Kathleen
Jackson, Kaleena
Harris, Todd R
et al.

Publication Date

2012-10-01

DOI

10.1152/ajpheart.00154.2012

Peer reviewed

Am J Physiol Heart Circ Physiol 303: H853–H862, 2012.
First published August 3, 2012; doi:10.1152/ajpheart.00154.2012.

Pharmacological inhibition of soluble epoxide hydrolase provides cardioprotection in hyperglycemic rats

Kathleen Guglielmino,[1] Kaleena Jackson,[1] Todd R. Harris,[2] Vincent Vu,[3] Hua Dong,[2] Gavin Dutrow,[3] James E. Evans,[3] James Graham,[4,5] Bethany P. Cummings,[4,5] Peter J. Havel,[4,5] Nipavan Chiamvimonvat,[6] Sanda Despa,[1] Bruce D. Hammock,[2] and Florin Despa[1]

[1]*Department of Pharmacology, University of California, Davis, California;* [2]*Department of Entomology, University of California, Davis, California;* [3]*Department of Molecular and Cellular Biology, University of California, Davis, California;* [4]*Department of Molecular Biosciences, School of Veterinary Medicine, University of California, Davis, California;* [5]*Department of Nutrition, University of California, Davis, California; and* [6]*Department of Internal Medicine, University of California, Davis, California*

Submitted 24 February 2012; accepted in final form 19 July 2012

Guglielmino K, Jackson K, Harris TR, Vu V, Dong H, Dutrow G, Evans JE, Graham J, Cummings BP, Havel PJ, Chiamvimonvat N, Despa S, Hammock BD, Despa F. Pharmacological inhibition of soluble epoxide hydrolase provides cardioprotection in hyperglycemic rats. *Am J Physiol Heart Circ Physiol* 303: H853–H862, 2012. First published August 3, 2012; doi:10.1152/ajpheart.00154.2012.—Glycemic regulation improves myocardial function in diabetic patients, but finding optimal therapeutic strategies remains challenging. Recent data have shown that pharmacological inhibition of soluble epoxide hydrolase (sEH), an enzyme that decreases the endogenous levels of protective epoxyeicosatrienoic acids (EETs), improves glucose homeostasis in insulin-resistant mice. Here, we tested whether the administration of sEH inhibitors preserves cardiac myocyte structure and function in hyperglycemic rats. University of California-Davis-type 2 diabetes mellitus (UCD-T2DM) rats with nonfasting blood glucose levels in the range of 150–200 mg/dl were treated with the sEH inhibitor 1-(1-acetypiperidin-4-yl)-3-adamantanylurea (APAU) for 6 wk. Administration of APAU attenuated the progressive increase of blood glucose concentration and preserved mitochondrial structure and myofibril morphology in cardiac myocytes, as revealed by electron microscopy imaging. Fluorescence microscopy with Ca^{2+} indicators also showed a 40% improvement of cardiac Ca^{2+} transients in treated rats. Sarcoplasmic reticulum Ca^{2+} content was decreased in both treated and untreated rats compared with control rats. However, treatment limited this reduction by 30%, suggesting that APAU may protect the intracellular Ca^{2+} effector system. Using Western blot analysis on cardiac myocyte lysates, we found less downregulation of sarco(endo)plasmic reticulum Ca^{2+}-ATPase (SERCA), the main route of Ca^{2+} reuptake in the sarcoplasmic reticulum, and lower expression of hypertrophic markers in treated versus untreated UCD-T2DM rats. In conclusion, APAU enhances the therapeutic effects of EETs, resulting in slower progression of hyperglycemia, efficient protection of myocyte structure, and reduced Ca^{2+} dysregulation and SERCA remodeling in hyperglycemic rats. The results suggest that sEH/EETs may be an effective therapeutic target for cardioprotection in insulin resistance and diabetes.

arachidonic acid pathway; hyperglycemia; diabetes; insulin resistance; calcium

HYPERGLYCEMIA is a major risk factor for the development of insulin resistance, type 2 diabetes mellitus (T2DM), and cardiovascular disease (CVD) (30). High blood glucose can damage the vasculature and affect heart structure and function (3–5, 8, 24, 46, 54). Hyperglycemia can also trigger inflammation and hypertension, which also contribute to CVD pathology (3–5, 8, 24, 30, 46, 54). The transition to T2DM generally accelerates pathological changes of the cardiovascular system (3–5, 8, 24, 30, 46, 54). Therefore, effective therapeutic strategies to limit or prevent CVD in patients with hyperglycemia require the control of blood glucose, blood pressure, and inflammation. Epoxyeicosatrienoic acids (EETs) are signaling molecules implicated in the modulation of blood pressure (25–28, 51), inflammatory cascades (22, 26, 27, 51), and glucose homeostasis (37, 38). Hence, controlling the endogenous levels of EETs appears as an effective strategy to protect the cardiovascular system against glucotoxicity. This can be achieved by preventing their degradation (27, 51) or through dietary supplementation. Intriguingly, dietary supplementation with docosahexaenoic acid (DHA), a naturally derived counterpart, improved mitochondrial function in the hypertrophied myocardium (31, 53). Apparently, EETs and DHA underlie similar mechanisms of cardioprotection that involve the activation of sarcolemmal and mitochondrial ATP-sensitive K^+ channels (35, 52).

Degradation of EETs can generally be prevented by inhibiting soluble epoxide hydrolase (sEH), an enzyme that converts EETs to dihydroxyeicosatrienoic acids (DHETs) (27, 51). Treatment with sEH inhibitors has demonstrated beneficial effects in animal models of high blood pressure (25, 26, 28), inflammation (10, 22, 26), myocardial injury (1, 23, 26, 41), ischemia-reperfusion (49, 50), pathological cardiac hypertrophy (26), and insulin resistance (37, 38). Hyperglycemic mice treated with sEH inhibitors showed improved insulin signaling and sensitivity (37, 38). On the basis that EETs appear to control biological processes that may be fundamental to cardioprotection, we hypothesized that modulating the endogenous levels of EETs using sEH inhibitors may protect the heart against structural and functional alterations induced by hyperglycemia. To test this hypothesis, we examined the structure and function of cardiac myocytes isolated from hyperglycemic rats treated with a sEH inhibitor versus untreated and normoglycemic, control rats. As an indicator of myocyte function, we measured Ca^{2+} cycling. Intracellular Ca^{2+} concentration ($[Ca^{2+}]_i$) is central to cardiac myocyte contractility and viability, and dysregulation of $[Ca^{2+}]_i$ plays an important role in the pathophysiology of heart disease (6), including diabetic cardiac disease (19, 32, 40, 45).

Address for reprint requests and other correspondence: F. Despa, Dept. of Pharmacology, Univ. of California, 451 Health Sciences Dr., Davis, CA 95616 (e-mail: fdespa@ucdavis.edu).

METHODS

In the present study, we used a rat model of hyperglycemia to test whether the inhibition of sEH can prevent molecular and cellular alterations of the myocardium.

Experimental animals. This investigation conformed with the National Institutes of Health *Guide for the Care and Use of Laboratory Animals* (NIH Pub. No. 85-23, Revised 1996) and was approved by the Institutional Animal Care and Use Committee of the University of California-Davis (UCD). For this study, we used the UCD-T2DM rat model of T2DM, which was obtained by breeding obese Sprague-Dawley rats with Zucker diabetic lean rats. UCD-T2DM rats exhibit polygenic adult onset obesity, insulin resistance, and inadequate pancreatic β-cell compensation, followed by the transition to hyperglycemia and T2DM (14, 15). Diabetes incidence, age of onset, longitudinal measurements of glucose, insulin, and lipids, and glucose tolerance were previously reported in Ref. 15. Data showing blunted insulin signaling, including Akt phosphorylation, in the liver, skeletal muscle, and adipose tissue in diabetic UCD-T2DM rats were reported in Ref. 14. Additional studies using the UCD-T2DM rat model to investigate the pharmacological and surgical treatment and prevention of T2DM were previously published in Refs. 14, 16, and 17. Here, nonfasting blood glucose concentrations were measured weekly starting at 2 mo of age. When the nonfasting blood glucose concentration was in the range of 150–200 mg/dl (8.3–11.1 mM) for two consecutive readings, rats were considered in a prediabetic stage. A total of 20 prediabetic male rats (15 ± 2 wk of age) were enrolled in this study, and a total of 10 age-matched male Sprague-Dawley rats (Charles Rivers Laboratory) were used as nondiabetic controls. Sprague-Dawley rats (Charles River Laboratory) were chosen as control animals since these animals were crossed to Zucker diabetic lean rats to generate the original UCD-T2DM rat model (15).

Treatment. Four prediabetic UCD-T2DM rats were euthanized before treatment. Cardiac myocytes isolated from these rats were examined for function and structure. In the present study, we used 1-(1-acetypiperidin-4-yl)-3-adamantanylurea (APAU) (UC1153, AR9281), a sEH inhibitor made using the methods of Jones et al. (29). Treatment with APAU improved endothelial function in animal models of T2DM, obesity, and hypertension (57). Rats in the sEH inhibitor treatment group (n = 10, 15 ± 2 wk old) received 1 ml APAU per liter of drinking water for 6 wk, starting from the onset of the prediabetic state. APAU was formulated in polypropylene glycol at a concentration of 10 mg/l with 30-min sonication and then added to drinking water at a final concentration of 10 mg/l. Rats had unrestricted access to water. Prediabetic rats in the untreated group (n = 6, 15 ± 2 wk old) received the same amount of polyethylene glycol, a neutral biocompatible polymer. Nonfasting blood glucose concentrations were measured weekly (morning time) in all rats with a glucometer (One Touch Blood Glucose Meter, LifeScan). One rat from the sEH inhibitor treatment group was found dead after 3 wk of treatment. No obvious symptoms of sickness were noticed in the behavior of the rat. At the end of the treatment period, rats were euthanized for cardiac myocyte isolation and subsequent functional and structural measurements.

Blood levels of APAU were assessed by liquid chromatography-tandem mass spectrometry (LC-MS/MS) in a subset of treated and control rats and ranged from 180 to 1,300 ng/ml, far in excess of what is required to inhibit the enzyme [$IC_{50} \approx 2$ ng/ml or 6 nM (55)]. The compound was not detected in control samples. APAU intake varied with blood glucose concentrations. Diabetic rats with blood glucose levels > 500 mg/dl received ~5 $mg \cdot kg^{-1} \cdot day^{-1}$ APAU and diabetic rats with blood glucose levels in the range of 200–500 mg/dl received ~3 $mg \cdot kg^{-1} \cdot day^{-1}$, whereas diabetic rats with blood glucose levels in the domain of 200–300 mg/dl as well as nondiabetic rats with blood glucose levels < 200 mg/dl received ~1 $mg \cdot kg^{-1} \cdot day^{-1}$. This is likely due to proportionally increased water intake as a result of hyperglycemia. Indeed, water intake increased from ~43 ml/day for nondiabetic rats to 150 ml/day for diabetic rats with blood glucose levels between 200 and 300 mg/dl and 250 ml/day for diabetic rats with blood glucose above 500 mg/dl.

EET level measurements. Analysis of EETs and their diols, DHETs, was performed by LC-MS/MS as previously described (58). Briefly, an Agilent 1200 SL LC series (Agilent, Palo Alto, CA) and an Agilent Eclipse Plus C18 2.1 × 150-mm, 1.8-μm column were used for EET separation. The mobile *phase A* was water with 0.1% acetic acid, whereas the mobile *phase B* was composed of acetonitrile-methanol [80:15 (vol/vol)] and 0.1% acetic acid. Gradient elution was performed at a flow rate of 250 μl/min. The injection volume was 10 μl, and the samples were kept at 4°C in the autosampler. Analytes were detected by negative MRM mode using a 4000 QTrap tandem mass spectrometer (Applied Biosystems Instrument, Foster City, CA) equipped with an electrospray ionization source (Turbo V). Calibration curves were generated by 10-μl injections of seven standards containing each analyte, *internal standard I*, and *internal standard II* for quantification purposes. Measurements were done of pancreas protein homogenates.

Cardiac myocyte isolation. Rats were anesthetized by an intraperitoneal injection of pentobarbital (~1 mg/g) and monitored for complete loss of reflexes, which was verified by firm foot pinch or loss of the blink reflex. When deep anesthesia was reached, hearts were quickly excised, placed on a Langendorff perfusion apparatus, and perfused with 1 mg/ml collagenase (18). When the heart became flaccid, the left ventricular tissue was cut into small pieces, dispersed, and filtered (18). The standard Tyrode solution used in these experiments contained (in mM) 140 NaCl, 4 KCl, 1 $MgCl_2$, 10 glucose, 5 HEPES, and 1 $CaCl_2$ (pH 7.4). All experiments were done at room temperature (23–25°C).

Transmission electron microscopy. For electron microscopy imaging (21), cardiac myocytes were isolated from treated (n = 4), untreated (n = 4), and healthy control (n = 4) rats and gently pelleted using a benchtop centrifuge (Eppendorf Centrifuge 5415D) operated for 3 min at 2,000 rpm. The pelleted samples were then loaded into 200-μm deep copper specimen carriers and rapidly frozen using a Leica EM-PACT2 high-pressure freezer. Frozen samples were then freeze substituted at −90°C for 50 h in anhydrous acetone containing 0.2% glutaraldehyde and 0.1% uranyl acetate using a Leica EM AFS device. Frozen samples were subsequently raised to −40°C at a rate of 5°C/h, kept at −40°C for 12 h, and warmed to 20°C at a rate of 10°C/h for infiltration and embedding in Eponate-12 resin with DMP-30 accelerator (Ted Pella). Resin-embedded samples were polymerized by heating at 70°C for 72 h, and blocks containing cardiac myocytes were cut into 70-nm-thick sections using a Leica Ultracut T microtome equipped with a Diatome 45° diamond knife. Serial sections were collected on slot grids covered with a 50-nm Formvar support film. Before being imaged, sections were poststained with 2% uranyl acetate in 70% methanol for 4 min. Grids were visualized on a transmission electron microscope (JEM-1230, JEOL) operated at 120 keV. Images of each section were recorded at ~2-μm defocus on a 2,048 × 2,048-pixel charge-coupled device camera (TVIPS, Gauting, Germany) and at nominal magnifications of either ×1,000 or ×2,500, yielding an effective pixel size of 11 or 4.4 nm, respectively.

Intracellular Ca^{2+} measurements. Myocytes were plated on laminin-coated coverslips, mounted on the stage of a fluorescence microscope, and loaded with fluo-4 AM (10 μmol/l). Fluo-4 was excited at 488 nm, and fluorescence was collected at 535 ± 30 nm. Ca^{2+} transients were elicited by field stimulation at frequencies between 0.2 and 2 Hz. Data are expressed as F/F_0, where F_0 is the fluorescence signal in resting myocytes and F is the measured fluorescence signal, to make the signal independent of the amount of dye loaded into myocytes. F_0 was measured for each cell during a stop in the pacing before the application of 10 mM caffeine (see Fig. 5*A*). Such normalization works only as long as resting $[Ca^{2+}]_i$ at which F_0 is measured is similar between groups. Initial tests (not shown) with the ratiometric indicator fura-2 revealed that resting $[Ca^{2+}]_i$ is indeed similar in

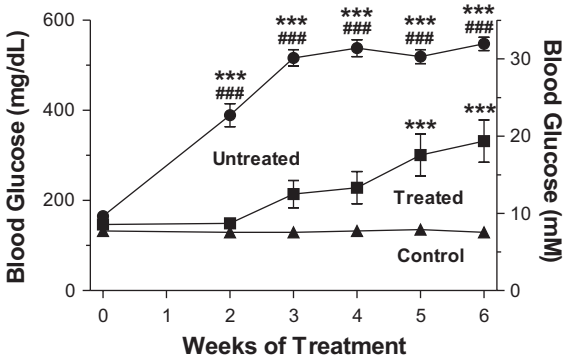

Fig. 1. 1-(1-Acetypiperidin-4-yl)-3-adamantanylurea (APAU) treatment attenuated the escalation of blood glucose levels in University of California-Davis (UCD)-type 2 diabetes mellitus (T2DM) rats. Blood glucose was measured weekly for the 6-wk treatment period ($n = 9$ APAU-treated rats, 6 untreated UCD-T2DM rats, and 10 nondiabetic control rats). ***$P < 0.001$ vs. the control group; ###$P < 0.001$ vs. the treated group (by two-way ANOVA).

myocytes from control and diabetic UCD-T2DM rats (untreated). Thus, we used diastolic fluo-4 F/F_0 as a measure of diastolic $[Ca^{2+}]_i$ and the difference between F/F_0 measured at systole and diastole as Ca^{2+} transient amplitude.

Immunochemistry. Isolated cardiac myocytes were lysed, and samples were centrifuged at 3,500 rpm to remove cellular components. Standard Western blot experiments were performed. Membranes were probed with primary antibodies against brain natriuretic peptide (BNP; Millipore), sarco(endo)plasmic reticulum Ca^{2+}-ATPase (SERCA; clone 2A7-A1, ABR), total phospholamban (PLB; Badrilla), PLB phosphorylated at Ser^{16} (Badrilla), and Na^+/Ca^{2+} exchanger (NCX, Millipore) as well as mitochondrial fission protein 1 (Fis1), dynamin-related protein 1 (DRP1), mitofusin 2 (Mfn2), and optic atrophy 1 (OPA1; all from Santa Cruz Biotechnology). Equal loading was verified by reprobing with anti-GAPDH (Thermo Scientific Pierce Antibodies).

Statistical analysis. Data are expressed as means ± SE. Statistical discriminations were performed using a two-tailed unpaired Student's *t*-test when two groups were compared, one-way ANOVA with Bonferroni's post hoc test when multiple groups were compared, and two-way ANOVA when multiple groups for multiple conditions were compared (as in Figs. 1, 4, *A* and *C*, and 5, *C* and *F*). *P* values of <0.05 were considered significant.

RESULTS

We assessed the course of blood glucose levels in treated versus untreated and control animals during the 6-wk treatment period. At the end of treatment, we examined cardiac myocyte morphology, Ca^{2+} cycling, and the level of expression of Ca^{2+} cycling proteins in all rats.

APAU improved glucose metabolism. The study was initiated when rats were in a prediabetic state, characterized by nonfasting blood glucose levels in the range of 150–200 mg/dl (8.3–11.1 mM) for two consecutive readings. Body mass was comparable for rats in the treated and untreated groups, both at the time of study initiation (572 ± 11 g for the untreated group vs. 562 ± 14 g for the treatment group) and after the 6 wk of treatment (572 ± 11 g for the untreated group vs. 596 ± 8 g for the treatment group). Two weeks after study initiation, all UCD-T2DM rats in the untreated group showed overt hyperglycemia and developed T2DM (nonfasting blood glucose level > 200mg/dl or 11.1 mM; Fig. 1). In contrast, the progression to hyperglycemia was considerably slower in APAU-treated UCD-T2DM rats (Fig. 1). Only half of the rats in the APAU treatment group had nonfasting blood glucose levels of >200 mg/dl (11.1 mM) and developed T2DM during the first 3 wk of treatment. In time, the inadequate pancreatic β-cell compensation in UCD-T2DM rats overcame the beneficial effects of APAU, leading to overt hyperglycemia. Thus, 80% of APAU-treated rats had developed diabetes at the end of the 6 wk of treatment. However, even the final blood glucose reading at the end of treatment was still significantly lower in treated versus untreated rats (Fig. 1). To assess the effect of APAU treatment on EET levels, we measured EETs and their corresponding diols, DHETs, in the pancreas from treated and untreated rats. There was a large increase of EETs in APAU-treated versus untreated rats (Table 1). Therefore, the EET-to-DHET ratio was greatly elevated in treated rats.

APAU reduced the structural alteration of cardiac myocytes. Ultrastructural examination of cardiac myocytes using serial section transmission electron microscopy (TEM) revealed that APAU could reduce hyperglycemia-mediated molecular alterations in the heart (Fig. 2). Cardiac myocytes from control rats has ellipsoidal-shaped mitochondria that were well organized into long, one mitochondrion-thick, continuous tracts nestled between adjacent myofibrils (Fig. 2, *A* and *D*). Myocytes from UCD-T2DM rats in the untreated group showed the altered mitochondrial morphology and mitochondrial fragmentation and clustering (Fig. 2, *B* and *E*) typical of cardiac dysfunction (13, 42–44). Mitochondrial fragmentation and clustering seemed to adversely affect the normal ultrastructure of adjacent myofibrils, as evidenced by the vertical shift of the Z-lines shown in Fig. 2*E*. In contrast, the majority of the mitochondria in myocytes from the APAU-treated group (Fig. 2, *C* and *F*) retained an ellipsoidal shape and were found in long, one mitochondrion-thick, continuous chains typical of rats in the control group. However, occasional mitochondrial clustering (white arrowhead in Fig. 2*C*) and myofibrillar disarray were also found in some myocytes from the APAU-treated group. We used automated contour modeling (Fig. 2, *G–I*) to measure the surface area of individual mitochondria and fat vacuoles from TEM images of myocytes from control, treated, and untreated groups. This analysis revealed larger individual fat vacuoles in myocytes from untreated UCD-T2DM rats compared with both control rats and treated UCD-T2DM rats (Fig. 3*A*). However, the total area occupied by fat vacuoles was similar in myocytes

Table 1. *Levels of EETs and inactive DHETs in the pancreas in untreated and 1-(1-acetypiperidin-4-yl)-3-adamantanylurea-treated rats*

	Treated Group	Untreated Group
EETs, ng/g protein		
14,15-EET	958 ± 151	114 ± 9*
11,12-EET	786 ± 181	109 ± 14
8,9-EET	354 ± 56	44 ± 11*
5,6-EET	1,737 ± 169	361 ± 53*
DHETs, ng/g protein		
14,15-DHET	10.8 ± 4.3	5.7 ± 1.6
11,12-DHET	16.5 ± 1.6	8.9 ± 0.7*
8,9-DHET	22.3 ± 5.5	21.7 ± 4.9
5,6-DHET	6.6 ± 2.0	4.2 ± 1.7

Values are means ± SE. EET, epoxyeicosatrienoic acid; DHET, dihydroxyeicosatrienoic acid. *$P < 0.05$.

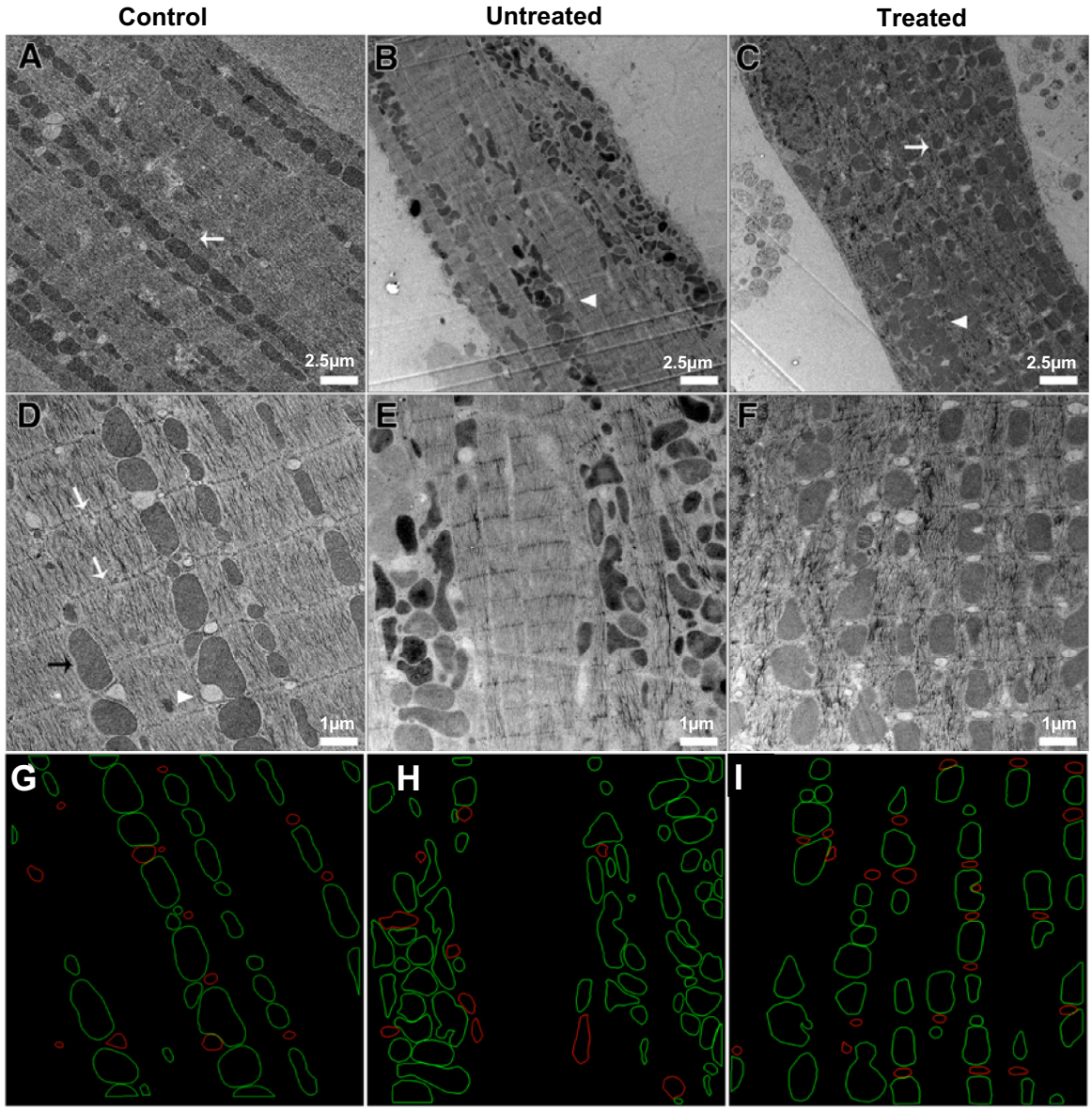

Fig. 2. Ultrastructural analysis of cardiac myocytes. *A–F*: transmission electron micrographs of isolated cardiac myocytes from control rats (*A* and *D*), untreated diabetic UCD-T2DM rats (*B* and *E*), and diabetic rats treated with soluble epoxide hydrolase inhibitor (*C* and *F*). Scale bars = 2.5 μm in *A–C* and 1.0 μm in *D–F*. White arrows in *A* and *C* indicate long, single tracks of mitochondria. White arrowheads in *B* and *C* indicate short, agglomerated mitochondria tracks. White arrows in *D* indicate the Z-lines for adjacent sarcomeres of a myofibril. The black arrow in *D* points to a single mitochondrion, and the white arrowhead indicates a fat deposit. *G–I*: contours for mitochondria (green) and fat vacuoles (red) in the images from *D–F*.

from treated and untreated rats and was larger than in control rats (Fig. 3*A*). The average size of cardiac mitochondria from untreated UCD-T2DM rats was significantly smaller than in control rats (Fig. 3*B*). However, the percentage of the cell occupied by mitochondria was similar (Fig. 3*B*). These data indicate mitochondrial fragmentation in myocytes from untreated UCD-T2DM rats. In contrast, cardiac mitochondria from treated UCD-T2DM rats had an average size similar to control rats (Fig. 3*B*). To further investigate this, we determined the expression level of two proteins associated with mitochondrial fission: mitochondrial Fis1 and DRP1. Both proteins were upregulated in untreated but not treated diabetic UCD-T2DM rats (Fig. 3, *C* and *D*). Surprisingly, the expression of Mfn2 and OPA1, proteins associated with mitochondrial fusion, was elevated in both treated and untreated UCD-T2DM rats versus control rats (Fig. 3, *C* and *D*). This suggests an increased turnover of mitochondrial fission and fusion processes in myocytes from untreated UCD-T2DM rats, which, as indicated by the TEM data, results in mitochondrial fragmentation.

APAU reduced the alteration of cardiac Ca^{2+} cycling in hyperglycemic rats. $[Ca^{2+}]_i$ is central to cardiac myocyte contractility and viability (6). $[Ca^{2+}]_i$ dysregulation plays an important role in the pathophysiology of heart disease (6), including diabetic cardiomyopathy (19, 32, 40, 45). Thus, we examined Ca^{2+} cycling in cardiac myocytes from age-matched treated and untreated UCD-T2DM rats and age-matched, healthy control rats.

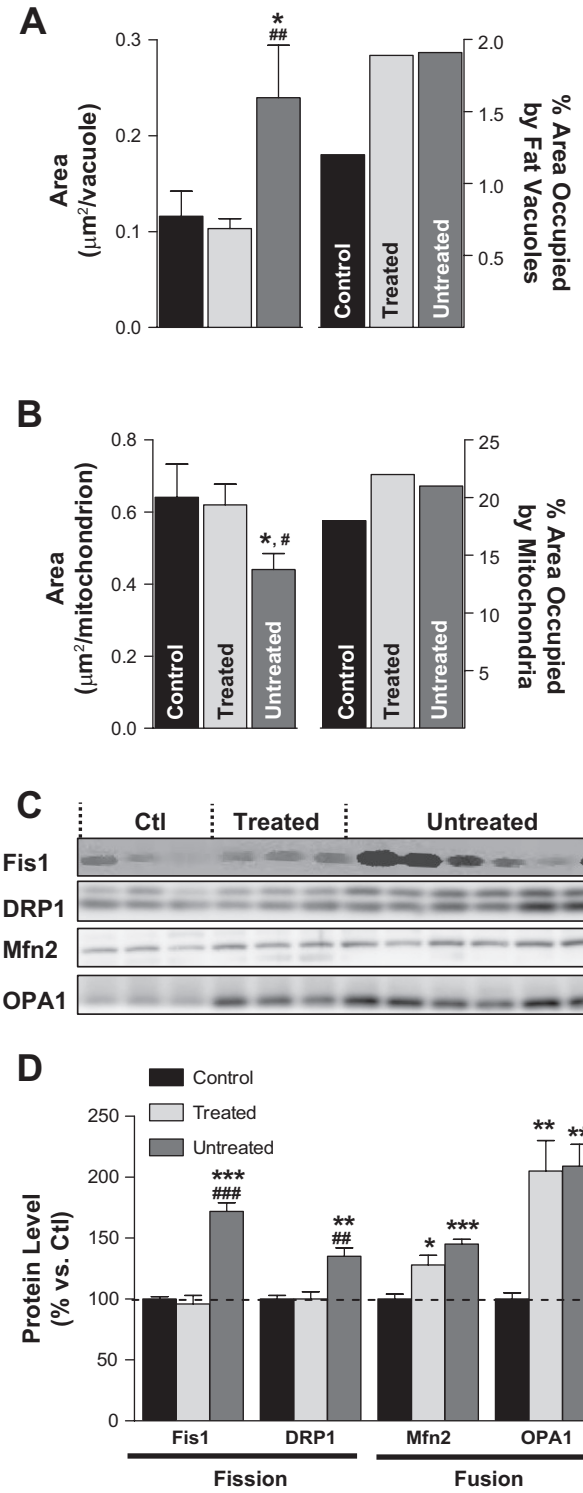

Fig. 3. Larger fat vacuoles and mitochondrial fragmentation in myocytes from untreated UCD-T2DM rats. *A*: average surface area of individual fat vacuoles (*left*) and the percent area they occupy (*right*) in myocytes from control (Ctrl), treated, and untreated rats. *B*: average surface area of individual mitochondria (*left*) and surface area occupied by mitochondria (as a percentage of myocyte area; *right*). Data in *A* and *B* were calculated from the transmission electron microscopy images. *C* and *D*: expression levels of proteins associated with mitochondrial fission [fission protein 1 (Fis1) and dynamin-related protein 1 (DRP1)] and fusion [mitofusin 2 (Mfn2) and optic atrophy 1 (OPA1)]. *$P < 0.05$ vs. the control group; **$P < 0.01$ vs. the control group; ***$P < 0.001$ vs. the control group; #$P < 0.05$ vs. the treated group; ##$P < 0.01$ vs. the treated group; ###$P < 0.001$ vs. the treated group.

Ca^{2+} transients were measured using the fluorescent indicator fluo-4 (Figs. 4 and 5). Myocytes were paced at 0.2, 0.5, 1, and 2 Hz until Ca^{2+} transients reached steady state (Fig. 5*A*). Pacing was then stopped for 10 s, and we applied 10 mM caffeine to empty the sarcoplasmic reticulum (SR) of Ca^{2+}. The amplitude of the caffeine-induced Ca^{2+} transient was used as a measure of SR Ca^{2+} content. At the start of APAU treatment, Ca^{2+} transient amplitude (Fig. 4*A*) and decay time (Fig. 4*B*) and diastolic $[Ca^{2+}]_i$ (Fig. 4*C*) measured in cardiac myocytes from UCD-T2DM rats were similar to control, non-

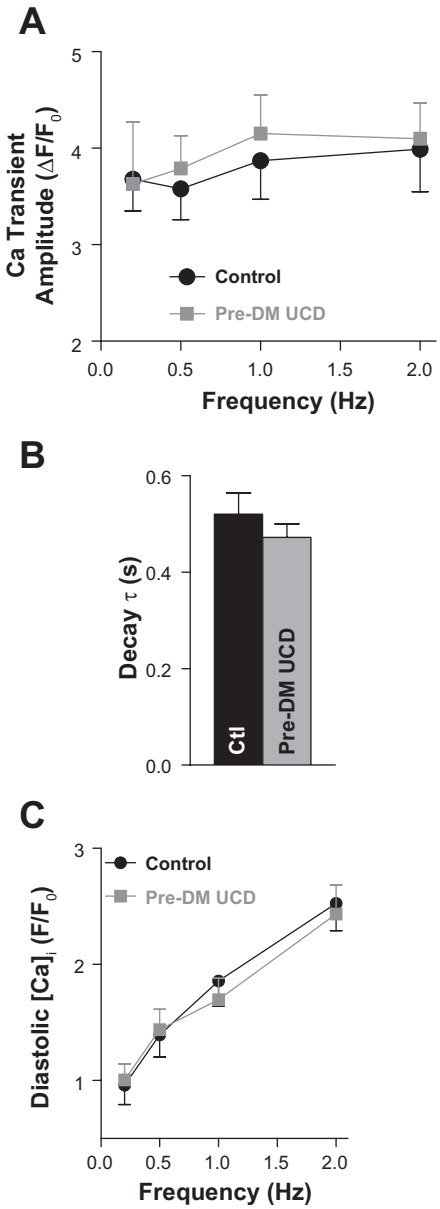

Fig. 4. Ca^{2+} transient characteristics are unaltered in UCD-T2DM rats at start of APAU treatment. *A*: Ca^{2+} transient amplitude in cardiac myocytes from prediabetic UCD-T2DM rats and control, nondiabetic rats. F/F_0, measured fluorescence signal (F)/fluorescence signal in resting myocytes (F_0). *B*: Ca^{2+} transient decay time (τ) in myocytes from prediabetic (pre-DM) UCD-T2DM rats and control, nondiabetic rats. *C*: diastolic intracellular Ca^{2+} concentration ($[Ca^{2+}]_i$) in myocytes from prediabetic UCD-T2DM rats and control, nondiabetic rats. $n > 20$ myocytes from 4 different animals/group. The rats used had an average age of 15 ± 2 wk.

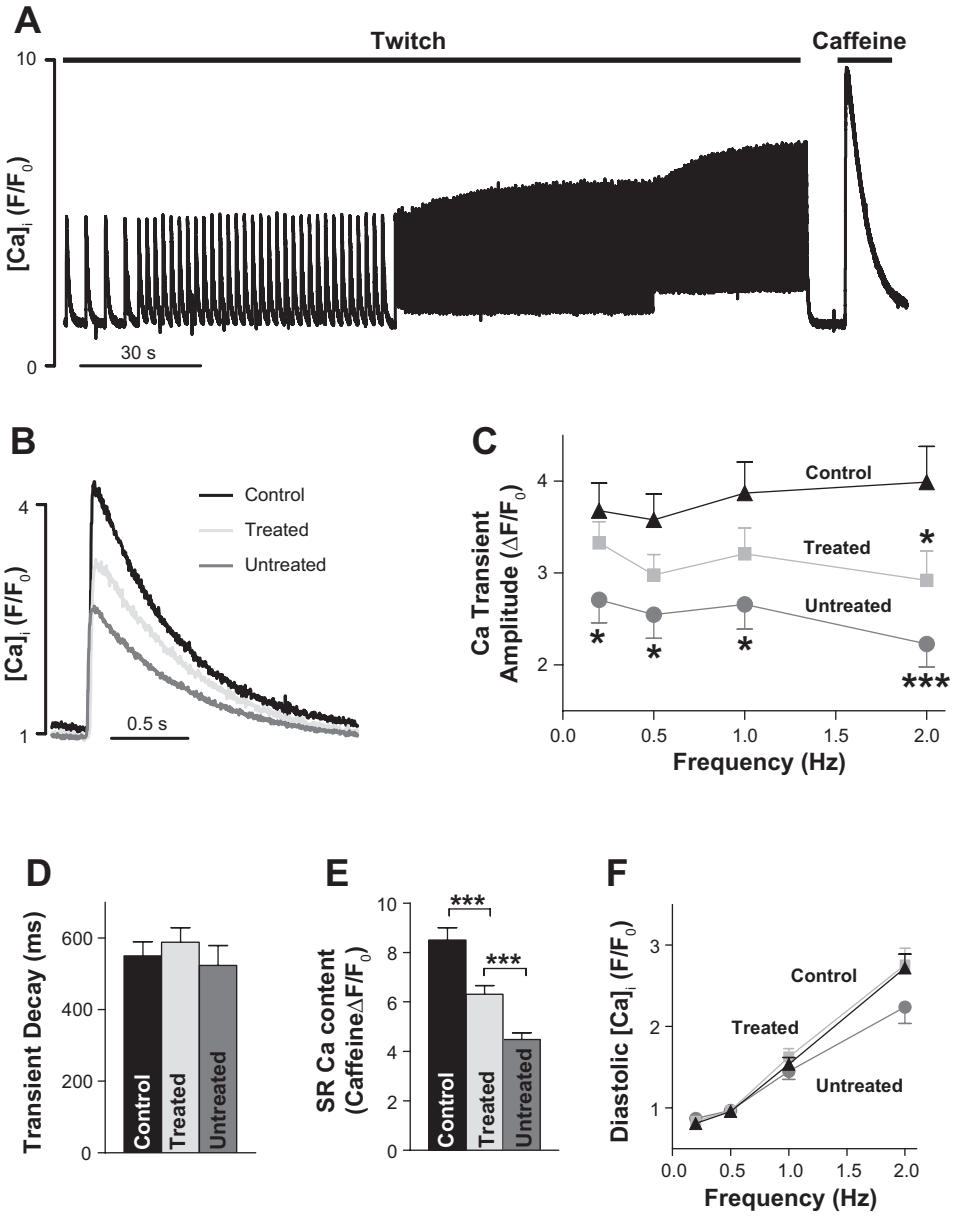

Fig. 5. APAU treatment partially prevents the decrease in Ca^{2+} transient amplitude and sarcoplasmic reticulum (SR) Ca^{2+} content in UCD-T2DM rats. *A*: representative example of Ca^{2+} transient and SR Ca^{2+} content measurements. Fluo-4 -loaded cardiac myocytes were paced with external electrodes at 0.2, 0.5, 1, and 2 Hz until Ca^{2+} transients reached steady state. After 2 Hz, pacing was stopped for 10 s, and we applied 10 mM caffeine to measure SR Ca^{2+} content. *B*: representative examples of Ca^{2+} transients in myocytes from nondiabetic control rats, untreated UCD-T2DM rats, and UCD-T2DM rats treated with APAU. Myocytes were paced at 0.5 Hz. *C–F*: mean Ca^{2+} transient amplitude (*C*), Ca^{2+} transient decay time (*D*), SR Ca^{2+} content (*E*), and diastolic $[Ca^{2+}]_i$ in cardiac myocytes from nondiabetic control rats, untreated UCD-T2DM rats, and UCD-T2DM rats treated with APAU. $n >$ 20 myocytes from 4 different animals/group. Measurements were done at the end of the 6-wk treatment period. $^*P < 0.05$ and $^{***}P < 0.001$ vs. the control group unless otherwise indicated.

diabetic rats. Hence, the slight rise of blood glucose did not alter cardiac myocyte Ca^{2+} regulation in prediabetic UCD-T2DM rats.

At the late T2DM stage, Ca^{2+} transients and SR Ca^{2+} content are drastically reduced, resulting in repressed contractility of the heart (32, 40, 45). This is generally attributed to the impaired glucose and lipid homeostasis in combination with vascular factors that lead to major cardiac remodeling (3, 4, 5, 8, 24, 30, 54). Indeed, cardiac myocytes isolated from UCD-T2DM rats that were not treated with APAU and therefore developed rapidly overt hyperglycemia (Fig. 1) had reduced Ca^{2+} transient amplitude (Fig. 4, *B* and *C*) and SR Ca^{2+} content (Fig. 5*E*), which are indicative of systolic heart dysfunction. Treatment with APAU partially prevented the reduction in both Ca^{2+} transient amplitude (by ~40%; Fig. 4, *B* and *C*) and SR Ca^{2+} content (by ~30%; Fig. 5*E*). In contrast to cardiac myocytes from control rats, myocytes from hyperglycemic UCD-T2DM rats showed a negative force-frequency relationship, particularly at higher stimulation frequencies (Fig. 5*C*). Treated and untreated UCD-T2DM rats did not show any alterations in Ca^{2+} transient relaxation (Fig. 5*D*) and diastolic Ca^{2+} (Fig. 5*F*), indicating normal diastolic function at this early stage of disease development.

APAU limited the pathological remodeling of cardiac myocytes in hyperglycemic rats. Alterations in the function and/or expression of proteins involved in Ca^{2+} cycling, particularly SERCA (11, 32, 40, 45), have been reported in various T2DM rodent models (11, 32, 40, 45). At the initial time point, before the start of the treatment, UCD-T2DM rats showed unaltered expression of SERCA (Fig. 6*A*). The development of overt hyperglycemia in untreated UCD-T2DM rats led to cardiac SERCA downregulation (Fig. 6, *C* and *D*), which may explain the reduction in SR Ca^{2+} content noted above (Fig. 5*E*). SERCA downregulation is a common occurrence in diabetic

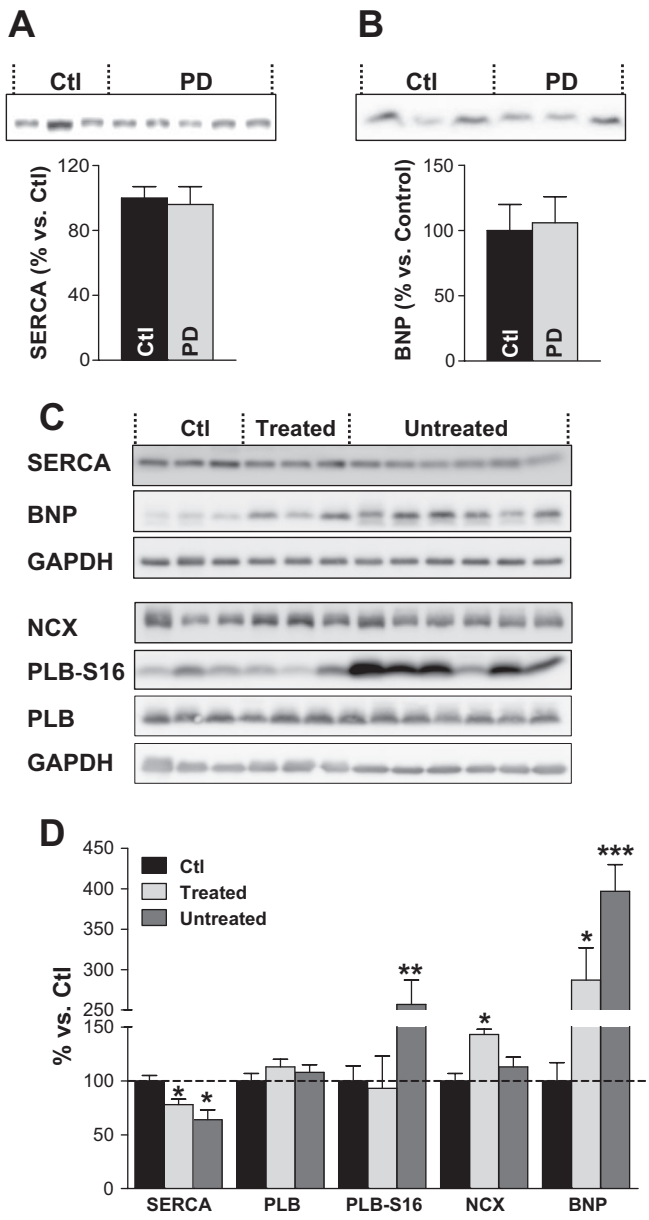

Fig. 6. APAU treatment mitigates the reduction in sarco(endo)plasmic reticulum Ca^{2+}-ATPase (SERCA) expression and the increase in brain natriuretic peptide (BNP) level in hearts from UCD-T2DM rats. *A* and *B*: at the time that APAU treatment was started (*time 0* in Fig. 1), SERCA (*A*) and BNP (*B*) levels in hearts from UCD-T2DM rats [prediabetic (PD)] were similar to those in hearts from control Sprague-Dawley rats. *C* and *D*: SERCA expression was significantly reduced, whereas the BNP level was increased, in hearts from both treated and untreated diabetic UCD-T2DM rats versus nondiabetic control rats. However, APAU treatment alleviated both SERCA downregulation and the increase in BNP expression. Phospholamban (PLB) expression was unchanged, but more PLB was phosphorylated at Ser^{16} (PLB-S16) in the untreated group. Na^+/Ca^{2+} exchanger (NCX) was significantly elevated in the APAU-treated group. *C*: representative examples; *D*: mean data. Western blots were run at least 4 times, and equal loading was verified with GAPDH. Measurements were done at the end of the 6-wk treatment period. $*P < 0.05$; $**P < 0.01$; $***P < 0.001$.

cardiomyopathy (46). Treatment with APAU partially limited the reduction in SERCA expression (Fig. 6, *C* and *D*), in agreement with its effect of mitigating the decrease in SR Ca^{2+} content. Intriguingly, APAU treatment favored an increase in NCX protein expression, the main route of Ca^{2+} extrusion (Fig. 6, *C* and *D*). Total expression of PLB, an endogenous SERCA inhibitor, was similar in all groups. However, more PLB was phosphorylated at Ser^{16} in the untreated group. Since PLB phosphorylation relieves SERCA inhibition, the increased PLB phosphorylation may, in part, mitigate the functional effect of SERCA downregulation.

APAU attenuated the expression of BNP in hyperglycemic UCD-T2DM rats. Increased natriuretic peptide levels are generally thought to reflect cardiac dysfunction and have been used as a "biomarker" of cardiac hypertrophy (20, 36, 48). The BNP level in cardiac myocytes from UCD-T2DM rats at the initial point of treatment was similar to control rats (Fig. 6*B*). However, the BNP level was four times higher in hearts from hyperglycemic UCD-T2DM rats versus age-matched control rats (Fig. 6*D*). This suggests hormonal alterations specific to the onset of cardiac hypertrophy in UCD-T2DM hyperglycemic rats. APAU treatment lowered the BNP level by ~30%, suggesting that the APAU-mediated cardioprotection may involve BNP signaling events, as suggested by recent work (12).

DISCUSSION

UCD-T2DM rats in the untreated group progressed rapidly to overt T2DM (Fig. 1) and demonstrated cardiac dysfunction at the cellular level, as shown by altered myocyte structure (Figs. 2 and 3), smaller Ca^{2+} transients and SR Ca^{2+} load (Fig. 5), myocyte remodeling (Fig. 6*B*), and prohypertrophic protein expression (Fig. 6). Inhibition of sEH slowed the development of T2DM (Fig. 1) and limited the morphological alterations of cardiac myocytes (Figs. 2 and 3), Ca^{2+} mishandling (Fig. 5), pathological remodeling of SERCA (Fig. 6*D*), and BNP expression (Fig. 6, *C* and *D*) in APAU-treated rats.

TEM micrographs showed altered mitochondrial morphology and mitochondrial fragmentation and clustering, typical for heart disease (13, 42–44), in myocytes from untreated UCD-T2DM rats. In agreement with this, we found elevated expression of proteins implicated in both mitochondrial fission and fusion, which suggests an increased turnover of these processes in hearts from the untreated group. APAU treatment alleviated mitochondrial fragmentation. In myocytes from the APAU-treated group, the majority of the mitochondria retained an ellipsoidal shape and the average size of the mitochondria and expression level of mitochondrial fission proteins were similar to the control group.

Ca^{2+} transient relaxation and diastolic Ca^{2+} were not altered in diabetic UCD-T2DM rats from either treated or untreated groups. Combined with reduced Ca^{2+} transient amplitude, this suggests that, in diabetic UCD-T2DM rats, systolic dysfunction occurs in the absence of diastolic dysfunction. This is somewhat surprising since in several other diabetic rodent models, including our T2DM rat model expressing human amylin (19), diastolic dysfunction precedes systolic dysfunction (19, 40, 45, 9). We found reduced SERCA expression in both treated and untreated diabetic UCD-T2DM rats. However, in the untreated group, the functional effect of SERCA downregulation may be mitigated by increased PLB phosphorylation at the Ser^{16} site, which disinhibits the existing SERCA pumps. In contrast, treated UCD-T2DM rats showed elevated NCX levels, which may also compensate for the reduction in SERCA.

Mechanism of APAU-induced cardioprotection. The main physiological role of sEH is to control the EET level, and pharmacological sEH inhibition has previously been shown to elevate EET blood levels (28). Indeed, we found significantly increased EETs levels in APAU-treated versus untreated rats. Thus, it is likely that the therapeutic effects of APAU observed here are the result of increased endogenous levels of EETs, which may elicit a multimodal mechanism of cardioprotection. APAU treatment and genetic sEH deletion have been previously shown to enhance glucose-stimulated insulin secretion and to improve insulin signaling and sensitivity in diabetic mice (37, 38). Thus, both mechanisms may contribute to reducing blood glucose levels in diabetic UCD-T2DM rats. It is clear that the attenuated hyperglycemia (Fig. 1) may play an important role in preserving cardiac myocyte structure (Fig. 2) and Ca^{2+} cycling (Fig. 5). On the other hand, EETs are involved in the activation of sarcolemmal and mitochondrial ATP-sensitive K^+ channels (35, 52), a critical mechanism of cardioprotection. Hence, APAU may induce a direct effect on cardiac Ca^{2+} handling (Fig. 5). The direct effect of EETs on the activation of mitochondrial ATP-sensitive K^+ channels may also explain the well-preserved cardiac mitochondrial structure in APAU-treated rats (Fig. 2). In addition, enhancing the EET level can generate antihypertensive and antiinflammatory effects (10, 22, 23, 25, 26, 28, 51) that may lessen the glucotoxicity on myocardial structure and function in APAU-treated rats.

Untreated hyperglycemic UCD-T2DM rats showed hormonal alterations specific to the onset of cardiac hypertrophy, as suggested by the increased BNP level (Fig. 6*B*). An increasing amount of experimental data have indicated that sEH inhibitors can attenuate cardiac hypertrophy (2, 34, 56). The process may involve BNP signaling events, as recently suggested (12). APAU-treated rats showed lower cardiac BNP concentrations compared with untreated rats (Fig. 6*C*), indicating that the cardioprotection provided by sEH inhibitors may indeed involve BNP signaling events.

While APAU seems a potent inhibitor of sEH, other sEH inhibitors may elicit a much improved inhibitory effect (33, 55). The new generation of inhibitors displays superior pharmacokinetics, absorption, distribution, metabolism, and excretion compared with APAU (33, 47). Hence, the cardioprotection against hyperglycemia can significantly be improved by using more potent sEH inhibitors. Nevertheless, the potency of sEH inhibitors may vary when the compounds are assayed against different mammalian sEH enzymes. For example, APAU is more potent against mouse and rat enzymes than the human enzyme and is a far weaker inhibitor of the canine enzyme (29, 33, 55). Extension of this study to other animal models of hyperglycemia and the use of other potent inhibitors may prove useful in optimizing the treatment for translational purposes.

Clinical relevance and study limitations. Hyperglycemia and T2DM are independent risk factors for adverse cardiovascular events. Clinical data have shown that a significant fraction of patients with T2DM do not achieve the optimum glycemic target goal (39). Although insulin treatment has been demonstrated to improve mechanisms of vasodilation and atherogenic lipid patterns and to reduce inflammatory markers predictive of heart disease, the risk of cardiovascular events remains high. Multimodal strategies to optimize glycemic control and provide cardioprotection across the phenotypic spectrum of diabetes are needed. Our study suggests that increasing the availability of endogenous EETs starting from prediabetes results in a slower progression of hyperglycemia, efficient protection of myocyte structure, and reduced Ca^{2+} dysregulation and SERCA remodeling in hyperglycemic rats. In the absence of a group of APAU-treated control, nondiabetic rats, we cannot determine whether this protection is mediated by attenuated hyperglycemia or is the direct effect of increased EETs on the heart. Further studies are also needed to assess the effectiveness of APAU if treatment is started after the onset of T2DM. The present results are limited by the lack of comparison of cardiac myocyte structure and function in UCD-T2DM rats treated with insulin.

In conclusion, pharmacological inhibition of sEH slows the progression of hyperglycemia and provides cardioprotection in a rat model of T2DM. The mechanisms by which sEH inhibitors can protect the heart from hyperglycemia seem to be multimodal and likely involve improved glucose regulation and direct actions on modulation of cardiac Ca^{2+} cycling. sEH could be an effective therapeutic target in the early stage of disease development, before the onset of full-blown T2DM.

GRANTS

This work was supported by American Heart Association Grant BGIA2220165, National Science Foundation Grant CBET-1133339, a Vision Grant from the University of California-Davis Health System (to F. Despa), and National Institutes of Health (NIH) Grant 1-R01-HL-109501 (to S. Despa). J. E. Evans acknowledges NIH Grant 5-RC1-GM-091755 for the ultrastructural analysis. P. J. Havel acknowledges support from NIH Grants R01-HL-075675, R01-HL-091333, R21-AT-003645, and RC1-DK-087307 for the development of the UCD-T2DM rat model. B. D. Hammock acknowledges funds from NIH Grants R01-ES-002710 and P42-ES-004699. B. D. Hammock is a George and Judy Marcus Senior Fellow of the American Asthma Foundation. T. R. Harris is supported by NIH Training Grant in Basic and Translational Cardiovascular Science T32-HL-86350.

DISCLOSURES

No conflicts of interest, financial or otherwise, are declared by the author(s).

AUTHOR CONTRIBUTIONS

Author contributions: K.G., K.N.J., T.R.H., V.V., H.D., G.D., J.E.E., J.L.G., B.P.C., S.D., and F.D. performed experiments; K.G., K.N.J., T.R.H., V.V., H.D., G.D., J.E.E., J.L.G., B.P.C., P.J.H., N.C., S.D., B.D.H., and F.D. approved final version of manuscript; T.R.H., H.D., J.E.E., B.P.C., S.D., and F.D. analyzed data; T.R.H., S.D., and F.D. interpreted results of experiments; T.R.H., J.E.E., B.P.C., P.J.H., N.C., S.D., B.D.H., and F.D. edited and revised manuscript; S.D., B.D.H., and F.D. conception and design of research; S.D. prepared figures; F.D. drafted manuscript.

REFERENCES

1. **Aboutabl ME, Zordoky BN, Hammock BD, El-Kadi AO.** Inhibition of soluble epoxide hydrolase confers cardioprotection and prevents cardiac cytochrome P450 induction by benzo(a)pyrene. *J Cardiovasc Pharmacol* 57: 273–281, 2011.
2. **Ai D, Pang W, Li N, Xu M, Jones PD, Yang J, Zhang Y, Chiamvimonvat N, Shyy JY, Hammock BD, Zhu Y.** Soluble epoxide hydrolase plays an essential role in angiotensin II-induced cardiac hypertrophy. *Proc Natl Acad Sci USA* 106: 564–569, 2009.
3. **Asghar O, Al-Sunni A, Khavandi K, Khavandi A, Withers S, Greenstein A, Heagerty AM, Malik RA.** Diabetic cardiomyopathy. *Clin Sci* 116: 741–760, 2009.
4. **Ashrafian H, Frenneaux MP, Opie LH.** Metabolic mechanisms in heart failure. *Circulation* 116: 434–448, 2007.
5. **Battiprolu PK, Gillette TG, Wang ZV, Lavandero S, Hill JA.** Diabetic cardiomyopathy: mechanisms and therapeutic targets. *Drug Discov Today Dis Mech* 7: e135–e143, 2010.

6. **Bers DM.** Calcium cycling and signaling in cardiac myocytes. *Annu Rev Physiol* 70: 23–49, 2008.
7. **Boron WF.** *Medical Physiology: a Cellular And Molecular Approach*. New York: Elsevier/Saunders, 2003.
8. **Boudina S, Abel ED.** Diabetic cardiomyopathy, causes and effects. *Rev Endocr Metab Disord* 11: 31–39, 2010.
9. **Bugger H, Abel ED.** Rodent models of diabetic cardiomyopathy. Molecular mechanisms for myocardial mitochondrial dysfunction in the metabolic syndrome. *Disease Models Mechanisms* 2: 454–466, 2009.
10. **Campbell WB, Gebremedhin D, Pratt PF, Harder DR.** Identification of epoxyeicosatrienoic acids as endothelium-derived hyperpolarizing factors. *Circ Res* 78: 415–423, 1996.
11. **Cesario DA, Brar R, Shivkumar K.** Alterations in ion channel physiology in diabetic cardiomyopathy. *Endocrinol Metab Clin North Am* 35: 601–610, 2006.
12. **Chaudhary KR, Batchu SN, Das D, Suresh MR, Falck JR, Graves JP, Zeldin DC, Seubert JM.** Role of B-type natriuretic peptide in epoxyeicosatrienoic acid-mediated improved post-ischaemic recovery of heart contractile function. *Cardiovasc Res* 83: 362–370, 2009.
13. **Chen Y, Liu Y, Dorn 2nd GW.** Mitochondrial fusion is essential for organelle function and cardiac homeostasis. *Circ Res* 109: 1327–1331, 2011.
14. **Cummings BP, Bettaieb A, Graham JL, Stanhope KL, Dill R, Morton GJ, Haj FG, Havel PJ.** Subcutaneous administration of leptin normalizes fasting plasma glucose in obese type 2 diabetic UCD-T2DM rats. *Proc Natl Acad Sci USA* 108: 1467–1475, 2011.
15. **Cummings BP, Digitale EK, Stanhope KL, Graham JL, Baskin DG, Reed BJ, Sweet IR, Griffin SC, Havel PJ.** Development and characterization of a novel rat model of type 2 diabetes mellitus: the UC Davis type 2 diabetes mellitus UCD-T2DM rat. *Am J Physiol Regul Integr Comp Physiol* 295: R1782–R1793, 2008.
16. **Cummings BP, Stanhope KL, Graham JL, Baskin DG, Griffen SC, Nilsson C, Sams A, Knudsen LB, Raun K, Havel PJ.** Chronic administration of the glucagon-like peptide-1 analog, liraglutide, delays the onset of diabetes and lowers triglycerides in UCD-T2DM rats. *Diabetes* 59: 2653–2661, 2010.
17. **Cummings BP, Strader AD, Stanhope KL, Graham JL, Lee J, Raybould HE, Baskin DG, Havel PJ.** Ileal interposition surgery improves glucose and lipid metabolism and delays diabetes onset in the UCD-T2DM rat. *Gastroenterology* 138: 2437–2446, 2010.
18. **Despa S, Bers DM.** Functional analysis of Na/K-ATPase isoform distribution in rat ventricular myocytes. *Am J Physiol Cell Physiol* 293: C321–C327, 2007.
19. **Despa S, Margulies KB, Chen L, Knowlton AA, Havel PJ, Taegtmeyer H, Bers DM, Despa F.** Hyperamylinemia contributes to heart dysfunction in obesity and diabetes, a study in humans and rats. *Circ Res* 110: 598–608, 2012.
20. **Ellmers LJ, Knowles JW, Kim HS, Smithies O, Maeda N, Cameron VA.** Ventricular expression of natriuretic peptides in $Npr1^{-/-}$ mice with cardiac hypertrophy and fibrosis. *Am J Physiol Heart Circ Physiol* 283: H707–H714, 2002.
21. **Evans JE, Renault L, Stahlberg H.** Structure determination using electron crystallography. In: *3D-Electron Microscopy in Life Sciences* (Handbook on DVD) (1st ed.), edited by Verkleij A, Orlova EV, Leis A. London, UK: 3DEM Network of Excellence, 2008, chapt. 9.
22. **Fleming I.** DiscrEET regulators of homeostasis: epoxyeicosatrienoic acids, cytochrome P450 epoxygenases and vascular inflammation. *Trends Pharmacol Sci* 28: 448–452, 2007.
23. **Gross GJ, Gauthier KM, Moore J, Falck JR, Hammock BD, Campbell WB, Nithipatikom K.** Effects of the selective EET antagonist, 14,15-EEZE, on cardioprotection produced by exogenous or endogenous EETs in the canine heart. *Am J Physiol Heart Circ Physiol* 294: H2838–H2844, 2008.
24. **Guha A, Harmancey R, Taegtmeyer H.** Nonischemic heart failure in diabetes mellitus. *Curr Opin Cardiol* 23: 241–248, 2008.
25. **Imig JD.** Epoxide hydrolase and epoxygenase metabolites as therapeutic targets for renal diseases. *Am J Physiol Renal Physiol* 289: F496–F503, 2005.
26. **Imig JD, Hammock BD.** Soluble epoxide hydrolase as a therapeutic target for cardiovascular diseases. *Nat Rev Drug Discov* 8: 794–805, 2009.
27. **Inceoglu B, Schmelzer KR, Morisseau C, Jinks SL, Hammock BD.** Soluble epoxide hydrolase inhibition reveals novel biological functions of epoxyeicosatrienoic acids (EETs). *Prostaglandins Other Lipid Mediat* 82: 42–49, 2007.
28. **Jiang H, Quilley J, Doumad AB, Zhu AG, Falck JR, Hammock BD, Stier CT Jr, Carroll MA.** Increases in plasma *trans*-EETs and blood pressure reduction in spontaneously hypertensive rats. *Am J Physiol Heart Circ Physiol* 300: H1990–H1996, 2011.
29. **Jones PD, Tsai HJ, Do ZN, Morisseau C, Hammock BD.** Synthesis and SAR of conformationally restricted inhibitors of soluble epoxide hydrolase. *Bioorg Med Chem Lett* 16: 5212–5216, 2006.
30. **Kannel WB, McGee DL.** Diabetes and cardiovascular disease. The Framingham study. *JAMA* 241: 2035–2038, 1979.
31. **Khairallah RJ, O'Shea KM, Brown BH, Khanna N, Des Rosiers C, Stanley WC.** Treatment with docosahexaenoic acid, but not eicosapentaenoic acid, delays Ca^{2+}-induced mitochondria permeability transition in normal and hypertrophied myocardium. *J Pharmacol Exp Ther* 335: 155–162, 2010.
32. **Lebeche D, Davidoff AJ, Hajjar RJ.** Interplay between impaired calcium regulation and insulin signaling abnormalities in diabetic cardiomyopathy. *Nat Clin Pract Cardiovasc Med* 5: 715–724, 2008.
33. **Liu JY, Tsai HJ, Hwang SH, Jones PD, Morisseau C, Hammock BD.** Pharmacokinetic optimization of four soluble epoxide hydrolase inhibitors for use in a murine model of inflammation. *Br J Pharmacol* 156: 284–296, 2009.
34. **Loch D, Hoey A, Morisseau C, Hammock BO, Brown L.** Prevention of hypertension in DOCA-salt rats by an inhibitor of soluble epoxide hydrolase. *Cell Biochem Biophys* 47: 87–98, 2007.
35. **Lu T, VanRollins M, Lee HC.** Stereospecific activation of cardiac ATP-sensitive K^+ channels by epoxyeicosatrienoic acids: a structural determinant study. *Mol Pharmacol* 62: 1076–1083, 2002.
36. **Luchner A, Stevens TL, Borgeson DD, Redfield M, Wei CM, Porter JG, Burnette JC Jr.** Differential atrial and ventricular expression of myocardial BNP during evolution of heart failure. *Am J Physiol Heart Circ Physiol* 274: H1684–H1689, 1998.
37. **Luo P, Chang HH, Zhou Y, Zhang S, Hwang SH, Morisseau C, Wang CY, Inscho EW, Hammock BD, Wang MH.** Inhibition or deletion of soluble epoxide hydrolase prevents hyperglycemia, promotes insulin secretion, and reduces islet apoptosis. *J Pharmacol Exp Ther* 334: 430–438, 2010.
38. **Luria A, Bettaieb A, Xi Y, Shieh GJ, Liu HC, Inoue H, Tsai HJ, Imig JD, Haj FG, Hammock BD.** Soluble epoxide hydrolase deficiency alters pancreatic islet size and improves glucose homeostasis in a model of insulin resistance. *Proc Natl Acad Sci USA* 108: 9038–9043, 2011.
39. **Mazzone T.** Diabetes and cardiovascular disease: intensive glucose lowering and cardiovascular disease prevention in diabetes: reconciling the recent clinical trial data. *Circulation* 122: 2201–2211, 2010.
40. **Netticadan T, Temsah RM, Kent A, Elimban V, Dhalla NS.** Depressed levels of Ca^{2+}-cycling proteins may underlie sarcoplasmic reticulum dysfunction in the diabetic heart. *Diabetes* 50: 2133–2138, 2001.
41. **Nithipatikom K, Moore JM, Isbell MA, Falck JR, Gross GJ.** Epoxyeicosatrienoic acids in cardioprotection: ischemic versus reperfusion injury. *Am J Physiol Heart Circ Physiol* 291: H537–H542, 2006.
42. **Ong SB, Subrayan S, Lim SY, Yellon DM, Davidson SM, Hausenloy DJ.** Inhibiting mitochondrial fission protects the heart against ischemia/reperfusion injury. *Circulation* 121: 2012–2022, 2010.
43. **Papanicolaou KN, Khairallah RJ, Ngoh GA, Chikando A, Luptak I, O'Shea KM, Riley DD, Lugus JJ, Colucci WS, Lederer WJ, Stanley WC, Walsh K.** Mitofusin-2 maintains mitochondrial structure and contributes to stress- induced permeability transition in cardiac myocytes. *Mol Cell Biol* 31: 1309–1328, 2011.
44. **Papanicolaou KN, Ngoh GA, Dabkowski ER, O'Connell KA, Ribeiro RF Jr, Stanley WC, Walsh K.** Cardiomyocyte deletion of mitofusin-1 leads to mitochondrial fragmentation and improves tolerance to ROS-induced mitochondrial dysfunction and cell death. *Am J Physiol Heart Circ Physiol* 302: H167–H179, 2012.
45. **Pereira L, Matthes J, Schuster I, Valdivia HH, Herzig S, Richard S, Gómez AM.** Mechanisms of $[Ca^{2+}]_i$ transient decrease in cardiomyopathy of *db/db* type 2 diabetic mice. *Diabetes* 55: 608–615, 2006.
46. **Razeghi P, Young ME, Cockrill TC, Frazier OH, Taegtmeyer H.** Downregulation of myocardial myocyte enhancer factor 2C and myocyte enhancer factor 2C-regulated gene expression in diabetic patients with nonischemic heart failure. *Circulation* 106: 407–411, 2002.
47. **Rose TE, Morisseau C, Liu JY, Inceoglu B, Jones PD, Sanborn JR, Hammock BD.** 1-Aryl-3-(1-acylpiperidin-4-yl)urea inhibitors of human and murine soluble epoxide hydrolase: structure-activity relationships, pharmacokinetics, and reduction of inflammatory pain. *J Med Chem* 53: 7067–7075, 2010.

48. **Schwartz K, Boheler KR, de la Bastie D, Lompre AM, Mercadier JJ.** Switches in cardiac muscle gene expression as a result of pressure and volume overload. *Am J Physiol Regul Integr Comp Physiol* 262: R364–R369, 1992.
49. **Seubert J, Yang B, Bradbury JA, Graves J, Degraff LM, Gabel S, Gooch R, Foley J, Newman J, Mao L, Rockman HA, Hammock BD, Murphy E, Zeldin DC.** Enhanced postischemic functional recovery in CYP2J2 transgenic hearts involves mitochondrial ATP-sensitive K^+ channels and p42/p44 MAPK pathway. *Circ Res* 95: 506–514, 2004.
50. **Seubert JM, Zeldin DC, Nithipatikom K, Gross GJ.** Role of epoxyeicosatrienoic acids in protecting the myocardium following ischemia/reperfusion injury. *Prostaglandins Other Lipid Mediat* 82: 50–59, 2007.
51. **Spector AA, Fang X, Snyder GD, Weintraub NL.** Epoxyeicosatrienoic acids (EETs): metabolism and biochemical function. *Prog Lipid Res* 43: 55–90, 2004.
52. **Spector AA, Norris AW.** Action of epoxyeicosatrienoic acids on cellular function. *Am J Physiol Cell Physiol* 292: C996–C1012, 2007.
53. **Stanley WC, Khairallah RJ, Dabkowski ER.** Update on lipids and mitochondrial function: impact of dietary n-3 polyunsaturated fatty acids. *Curr Opin Clin Nutr Metab Care* 15: 122–126, 2012.
54. **Taegtmeyer H, Stanley WC.** Too much or not enough of a good thing? Cardiac glucolipotoxicity versus lipoprotection. *J Mol Cell Cardiol* 50: 2–5, 2011.
55. **Tsai HJ, Hwang SH, Morisseau C, Yang J, Jones PD, Kasagami T, Kim IH, Hammock BD.** Pharmacokinetic screening of soluble epoxide hydrolase inhibitors in dogs. *Eur J Pharm Sci* 40: 222–238, 2010.
56. **Xu D, Li N, He Y, Timofeyev V, Lu L, Tsai HJ, Kim IH, Tuteja D, Mateo RK, Singapuri A, Davis BB, Low R, Hammock BD, Chiamvimonvat N.** Prevention and reversal of cardiac hypertrophy by soluble epoxide hydrolase inhibitors. *Proc Natl Acad Sci USA* 103: 18733–18738, 2006.
57. **Zhang LN, Vincelette J, Chen D, Gless RD, Anandan SK, Rubanyi GM, Webb HK, MacIntyre DE, Wang YX.** Inhibition of soluble epoxide hydrolase attenuates endothelial dysfunction in animal models of diabetes, obesity and hypertension. *Eur J Pharmacol* 654: 68–74, 2011.
58. **Yang J, Schmelzer K, Georgi K, Hammock BD.** Quantitative profiling method for oxylipin metabolome by liquid chromatography electrospray ionization tandem mass spectrometry. *Anal Chem* 81: 8085–8093, 2009.